




Three-channel electrical impedance spectroscopy for field-scale root phenotyping

Luca Peruzzo¹  | Xiuwei Liu² | Chunwei Chou¹ | Elisa B. Blancaflor³ |
 Haijun Zhao³ | Xue-Feng Ma³  | Benjamin Mary^{1,4}  | Veronika Iván⁴ |
 Maximilian Weigand⁵ | Yuxin Wu¹

¹ Earth and Environmental Sciences Area, Lawrence Berkeley National Laboratory, Berkeley, CA, 94720, USA

² Center for Agricultural Resources Research, Chinese Academy of Sciences, Shijiazhuang, Hebei, 050021, China

³ Noble Research Institute, LLC, Ardmore, OK, 73401, USA

⁴ Dip. di Geoscienze, Univ. degli Studi di Padova, Padova, 35131, Italy

⁵ Section Geophysics, Institute of Geosciences, Univ. of Bonn, Bonn, 53115, Germany

Correspondence

Luca Peruzzo, Earth and Environmental Sciences Area, Lawrence Berkeley National Laboratory, CA 94720, USA.
 Email: lperuzzo@lbl.gov

Assigned to Associate Editor Daniel Northrup.

Abstract

Electrical impedance spectroscopy has long been considered a promising technique for noninvasive, in-situ root investigation because of its sensitivity to anatomy and physiology. However, the complexity of the root system and its coupling with stem and soil have hindered the signal interpretation and methodological upscaling to field applications. This study addresses these key issues by introducing three-channel acquisitions and their interpretation through Cole–Cole fitting. This solution could successfully decouple the impedance response of stem, roots, and soil, as well as provide convenient parametrization and comparison of their impedance signals. The methodological solution was tested on 80 wheat (*Triticum aestivum* L.) and 10 pecan [*Carya illinoensis* (Wangenh.) K. Koch] plants, the first extensive and field investigation. The investigation provided evidence of (a) proximal current leakage in herbaceous root systems, extending recent laboratory results and previous indirect field studies. (b) Major role of the plant stem, which has been a substantial concern raised in numerous studies. (c) Minor contribution from the soil, addressing the doubts on the comparability of results obtained in different soil conditions. All together, these evidences lead to indirect correlations between impedance signals and root traits. The explored solution is expected to support the adoption of the impedance spectroscopy, in line with the diffusion of multichannel impedance meters and growing interest in root physiology and phenotyping.

1 | INTRODUCTION

Today's most pressing environmental, social, and economical issues remind us that plants have underpinned and driven the evolution of Life and Environment. These same issues also

force us to acknowledge plant roots as the hidden protagonist, whose functioning remains difficult to access and challenging to understand. Consequently, there is a growing interest in in-situ and non-invasive root phenotyping methods to overcome the limitations of traditional destructive root investigation methods, such as soil coring, profiling, and shovelomics (Atkinson et al., 2019; Zhao et al., 2019).

Abbreviations: EIS, electrical impedance spectroscopy; iCSD, inversion of current source density; SRS, stem–root–soil.

This is an open access article under the terms of the [Creative Commons Attribution](https://creativecommons.org/licenses/by/4.0/) License, which permits use, distribution and reproduction in any medium, provided the original work is properly cited.

© 2021 The Authors. *The Plant Phenome Journal* published by Wiley Periodicals LLC on behalf of American Society of Agronomy and Crop Science Society of America

Electrical impedance spectroscopy (EIS) is a well established and widely used technique for characterizing biological materials, including anatomy, physiology, and pathology (Bera, 2014; Jaffrin & Morel, 2008). Plant research has long been applying the EIS method to plant physiology and in situ root investigations (Hayden et al., 1969; Volkov, 2006). This research effort is in line with the known sensitivity of impedance methods to fluid pathways and chemistry, and presence and continuity of dielectric membranes (Bera, 2018). The sensitivity to these crucial physiological aspects is particularly evident thanks to the frequency-dependent impedance response of the plant tissues. Compared to single-frequency or direct current (DC) analyses, EIS investigations better account for the complexity of the plant tissues, such as the coexistence of multiple current and fluid pathways (Ehosioko et al., 2020). In particular, the distinction between low-frequency apoplastic pathway and high-frequency symplastic pathway is now better understood (Jócsák et al., 2019; Zhao et al., 2019).

The EIS method has been applied on both trimmed roots and the whole stem–root–soil (SRS) continuum. In the former, trimmed-root applications, all the electrodes are connected to the investigated root section (Mary et al., 2017). In the latter, stem-injection applications, the current is injected into the plant stem and returned in the soil nearby, inducing a current flow through the investigated root system (Figure 1). The EIS studies have been successful in the physiological investigation of trimmed roots, where the current pathways are more constrained (Ehosioko et al., 2018; Hayden et al., 1969). On the contrary, full interpretations of the stem-injection results remain hindered and debated due to uncertainties on the current pathways in the SRS electrical continuum (Cseresnyés et al., 2020; Urban et al., 2011).

The stem-injection signals only depend on the sections of the root system investigated by the current flow. Hence, the main concern is the possible current leakage from the proximal part of the root system. Repo et al. (2005) performed hydroponic experiments with willow plants and reported that “We do not know which proportion of the change in resistances is due to the increase of root mass or root surface area and which, if any, is due to the change in stem or stem/solution interface during growing period.” Cao et al. (2010) also performed hydroponic experiments with willow (*Salix* spp.) plants and found that “the electrical resistance remained approximately the same when the stem with or without the root was in contact with the solution”; see also their Figure 4. Dietrich et al. (2012) revised Dalton’s model (Dalton, 1995) based on trimming experiments in hydroponic conditions with barley (*Hordeum vulgare* L.) plants. While the proposed model allowed impedance contributions from the entire root system, the authors assessed that the impedance response was dominated by the plant tissue between the stem electrode and solution surface, particularly

Core Ideas

- Three-channel and Cole–Cole fitting can target the impedance response of the root system.
- First field scale impedance spectroscopy campaign, 80 wheat and 10 pecan plants.
- Dominant role of stem and proximal roots on the impedance response.
- Indirect correlation between impedance signals and root traits.
- Minor soil influence even in clayey soils.

by the cross-sectional area at the surface interface. Urban et al. (2011) investigated the possible causes for the above and concluded that most of the injected current leaks to the soil from the very proximal part of the investigated root system.

Despite the growing evidence on the possible EIS limitations in root investigations, the need for advancing root phenotyping have motivated numerous studies that supported the use of EIS. Even the above studies, with the exception of Urban et al. (2011), supported the use of the EIS method in light of promising correlations with root traits. A collection of these works is presented in Dietrich et al. (2012), their Table 1; Postic and Doussan (2016), their Table 3; and Jócsák et al. (2019). Together these studies report about 50 works focusing on roots, and as many focusing on the aerial parts of the plant, leading to an apparent contradiction. The main aspect hindering a comprehensive interpretation of the EIS results is the natural complexity of the root–soil system, specifically, the inter- and intraspecific variability of the pathways of water/ion and current. For example, hydroponic conditions are known to increase ion mobility through the root and could have contributed to the proximal current leakage in the above hydroponic studies (Enstone & Peterson, 2005; Redjala et al., 2011; Tavakkoli et al., 2010; Zimmermann & Steudle, 1998). Similar strong variability exists between herbaceous and woody roots, the former being prone to proximal current leakage (Schreiber, 2010).

In order to address the complexity and variability of the current pathways, recent studies presented a solution for imaging the current pathways in the SRS continuum based on the inversion of current source density (iCSD). Peruzzo et al. (2020) corroborated the proximal-root current leakage in crop roots (maize [*Zea mays* L.] and cotton [*Gossypium hirsutum* L.], in hydroponic and soil conditions). Mary et al. (2018, 2019, 2020) supported more distal current pathways in grapevines (*Vitis* spp.) and orange trees (*Citrus* spp.) (soil/field conditions). Mary et al. (2020) also highlighted the irrigation influence on the current pathways in the SRS continuum. In light of the newly available evidence, Peruzzo et al. (2020) discussed

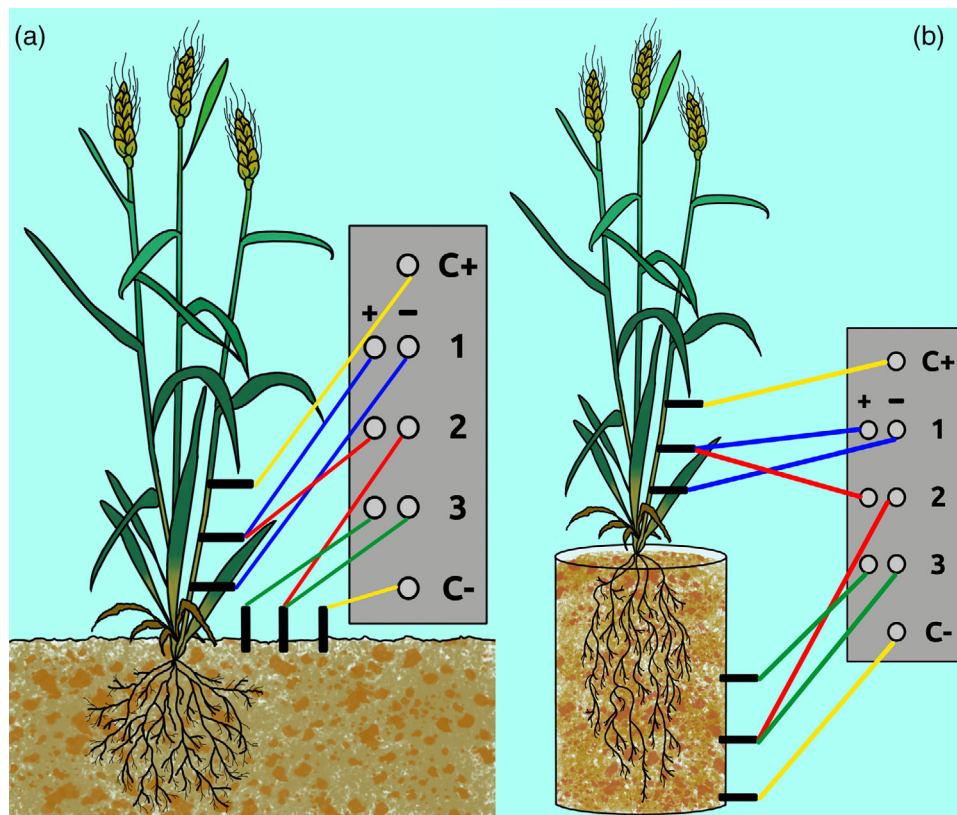


FIGURE 1 Configuration of the electrodes and electrical impedance spectroscopy (EIS) channels for the (a) field and (b) hoop house acquisitions. The figure is not to scale. In the field, the interspace of the soil electrodes is 1 m, and 1 m is also the distance between the plant and the closest electrode. In the hoop house, the interspace is 20 cm, and there are 20 cm also between the plant and the first-shallowest electrode

current pathways in plant tissues, including the influence of growing conditions and interspecies variability, as well as the differences between herbaceous and woody roots. These results confirmed the importance of addressing the relative role of soil and stem during stem-injection investigations of the SRS electric continuum.

While the iCSD method supports the understanding of current pathways in the SRS continuum, it requires geophysical-imaging knowledge and instrumentation. With regard to stem-injection EIS studies, the iCSD imaging significantly differs from the EIS concepts and requires specific resistivity meters for tomographic applications (Binley & Kemna, 2005; Cassiani et al., 2015). Consequently, methodological advances to address the limitation of the present EIS setup remain desirable.

The EIS stem-injection investigations rely on a single acquisition channel (i.e., channel 2 in Figure 1). With a single channel, the need to target a specific part of the SRS continuum has been addressed at the experimental designed level. Hydroponic experiments have been performed to reduce the uncertainty associated with the growing medium, see Ozier-Lafontaine and Bajazet (2005), Dalton (1995), McBride et al. (2008), and citations above. Here, water offers significant advantages compared to soil because of its homogeneity

and negligible impedance response in the typical investigated frequency range (<20 kHz). Hermanská et al. (2015) recently confirmed the unresolved issue of discerning the impedance response of roots and growing medium in field wheat (*Triticum aestivum* L.) experiments. The stem contribution has been addressed by changing the height of the stem electrode and evaluating the impact on the overall response of the SRS continuum (Dalton, 1995; Ozier-Lafontaine & Bajazet, 2005). Similarly, the soil electrodes (both potential and current) can be moved relative to the plant stem to obtain the *impedance curve*, from which the extension of the root system is estimated (Aubrecht et al., 2006; Cermák et al., 2013; Urban et al., 2011). Finally, a *subtractive* solution was used to target the root response; during the hydroponic experiments the roots were submerged in water and progressively trimmed, linking the induced variations of the root system to the changes in the SRS impedance response (Dietrich et al., 2012). Similarly, Cermak et al. (2006) included root severing experiments in their field campaign investigating the relationship between root impedance response and traits.

A second aspect central to the applicability and upscaling of the EIS is the analysis of the impedance spectra. The EIS spectra are typically described by 10s of data points in the frequency range from mHz to kHz (Mancuso, 2012).

Different approaches have been used to synthesize the EIS spectra and obtain parameters with particular physiological meaning and/or statistically effective in predicting root traits. Magnitude and phase at one or few relevant frequencies (e.g., peak frequency) are used because of their relative simplicity. However, this approach provides a lossy synthesis/description of the spectra and it is sensitive to the noise of the considered data points. To overcome these limitations, equivalent circuit and phenomenological models (e.g., Cole–Cole) are used to fit the EIS spectra or in decomposition schemes (Dietrich et al., 2012; Weigand & Kemna, 2016). These approaches allow the description of features in the EIS spectra while limiting the number of parameters, which are also less sensitive to the data noise as they depend on multiple data points.

The introduced need for improved stem-injection investigations has been acknowledged by previous EIS works and corroborated by the recent iCSD results. A consequence of the methodological limitations and underlying need for design-specific investigations is the lack of extensive field campaigns and industry adoption. Nonetheless, the increasing availability of multichannel impedance meters and better understanding on plant impedance response support the development and upscaling of EIS for studying roots. Our goal is to combine 3-channel EIS measurements with Cole–Cole fitting to distinguish and further analyze the root impedance response, allowing upscaling to extensive field applications. We apply the proposed methodological advances to the first field-scale EIS campaign, counting 80 wheat (*Triticum aestivum* L.) plants (field and hoop house) and 10 pecan [*Carya illinoensis* (Wangenh.) K. Koch] plants. Thanks to its methodological contribution and large field scale, this study provides new insight on the interpretability and validity of the EIS in agricultural applications. To strengthen our interpretations, EIS impedance data are compared with root data from soil coring and root excavation.

2 | MATERIAL AND METHODS

2.1 | Field and hoop house

The experiments were performed at the Noble Research Institute (Ardmore, OK) during the 2018 growing season. Both field and hoop house experiments were performed. A total of 80 wheat plants were grown and investigated, 40 in the hoop house and 40 in the field. In addition to the measurements on wheat plants, 10 pecan plants were included in the hoop house experiments to provide a comparative woody root, single stem dataset.

The 40 field plants were sown on a regular grid with 1 m interspace. The interspace was chosen to allow independent growth, convenient experimental access, and individual excavation and coring of the roots. The soil at the field site is Hay-

den clay (fine, montmorillonitic, thermic Udic Chromustert). The soil has an average pH of 6.7 and organic matter content of 34 g kg⁻¹ (Butler et al., 2012). The local moisture regime and soil properties prevented significant water stress during the growing season. Plants were sown in September and harvested in June. Experiments were conducted on 26 April, during the grain-filling stage, milk stage. The cultivated varieties of the field plants were Duster, NF101, and TAM111.

The 40 hoop house plants were grown individually in columns of height 1.7 m and diameter 25 cm. Plants were sown in mid-September and harvested in June. The EIS measurements were performed on 3 May, 1 wk after the field measurements, during the grain-filling stage, milk stage. The hoop house wheat plants were exposed to different irrigation regimes: 20 plants were fully irrigated while 20 were exposed to water deficit conditions (50% deficit). Additional variability was induced by cutting operations: nodal root cuts were performed on five plants and tiller cuttings on another five plants. The cultivated varieties of the hoop house were Garrison, Triumph64, Tascosa, TAM111, and TAM107.

2.2 | Electrical impedance spectroscopy acquisitions

For the impedance acquisitions, we used a Portable Spectral Induced Polarization by Ontash & Ermac (PSIP) impedance meter. Impedance measurements were performed at 41 logarithmically spaced frequencies from 10 Hz to 20 kHz. The injection voltage was limited to 5 V to avoid high intensity currents that could damage the plant tissues, thus affecting the impedance response (Aubrecht et al., 2006). Shielded cable of 1.5 m were used to connect the electrodes in the hoop house. In the field, the same cables were used for the plant electrodes, while longer cables (2–4 m) were used to allow the positioning of the soil electrodes.

Silver/silver chloride electrodes were obtained by cutting 2-mm thick silver wire into 1-cm pieces and bleaching them for 6 h. The three stem electrodes were sharpened and mounted on a small clamp as in a pair of hole punch pliers, allowing a more convenient and stable installation of the electrodes. The clamp also distributes the weight of the electrode and cable on a wider section of the stem, preventing damages to the plant. The size of the electrodes necessarily caused the piercing of multiple cells, the resulting injection involved both extra- and intra-cellular spaces. The impedance measurements were performed immediately after the positioning of the electrodes to limit the impact of the electrodes on the plant tissues and their impedance response, particularly with regard to the cell piercing. The electrochemical stability of the silver/silver chloride electrodes excluded possible alteration of the electrodes during the relatively short and non-demanding experimental procedures. No wearing of the electrodes was observed.

Figure 1 shows the 3-channel setup used for the EIS measurements. The current electrodes (C+ and C−) induce an electric current flow from the injection electrode in the stem to the return electrode in the soil near the plant. The electric current initially flows through the plant stem section below the injection point. Once the current reaches the soil surface, it distributes among the different possible pathways in the root–soil system on the basis of their electrical impedance.

The current electrode in the stem was positioned at a height of 6.0 ± 0.5 cm from the soil surface. The electrodes for the potential measurement in the stem were positioned at 3.0 ± 0.5 cm and 0 cm (i.e., soil surface) height. The stem morphology and its variability hindered more accurate positioning of the stem electrodes.

The positioning of the soil electrodes necessarily depended on the type of experiment. In field experiments the three soil electrodes were radially aligned relative to the plant. The two potential electrodes were positioned on the soil surface at 1 and 2 m from the plant. The current return electrode was placed at 3 m from the plant. Such a distance was based on initial tests and provided the best compromise between current penetration and soil impact on the measurements. A closer return electrode would force proximal/shallow current leakage and consequently hinder an objective investigation of the SRS continuum (Peruzzo et al., 2020).

For the experiment in the hoop house columns the soil electrodes were positioned as shown in Figure 1, both for wheat and pecan plants. Stem electrodes were positioned as in the field experiments. The soil electrodes were positioned from the column side on a vertical line to increase the signal strength. The two soil electrodes of potential were positioned at a depth of 20 and 40 cm, the return current electrode was installed at a depth of 60 cm.

In the 3-channel configuration, each dipole is sensitive to a different portion of the SRS electrical continuum (Figure 1). Channel 1 (C1) only depends on the impedance response of the stem section interested by the current flow, between C1+ and C1−. Channel 2 (C2) measures the overall response of the SRS continuum, that is, from the stem potential C2+ to the potential electrode C2− in the soil. Channel 3 (C3) only depends on the soil impedance response of the soil, between C3+ and C3−. Therefore, C1 and C3 provide direct access to the response of stem and soil, and together they allow decoupling the root response from C2.

We applied the above setup to all the grown wheat and pecan plants, for a total of 90 three-channel EIS datasets. In addition, we randomly selected four field plants and five tillers from each of them to investigate EIS response differences among the tillers of the same plant. These 20 datasets were acquired on the same day and with the same approach as the other field experiments.

2.3 | Cole–Cole analysis of plant tissues

The Cole–Cole fitting routine was based on Weigand and Kemna (2016) and written in Python, using the *least_squares* function provided by the SciPy library, see also Rucker et al. (2017). In particular, the Pelton resistivity formulation of the Cole–Cole model was used (Pelton et al., 1978). See Tarasov and Titov (2013) and Macnae (2015) for details on the relationship between the Cole–Cole and Pelton models. While a model formulation with multiple additive Cole–Cole terms was possible, the specific routine was limited to a single Cole–Cole term. The single-term choice is in line with the impedance response of roots and avoids unnecessary and poorly determined Cole–Cole terms (Ehosioko et al., 2018; Mary et al., 2017).

The single-term Pelton model is

$$Z(\omega) = R_0 \left[1 - m \left(1 - \frac{1}{1 + (i\omega\tau)^c} \right) \right] \quad (1)$$

where R_0 is the DC (low-frequency) resistance [Ω], m is the chargeability [–], τ is the relaxation time [s], and c [–] is the Cole–Cole exponent describing the broadness of the relaxation time distribution.

The four Cole–Cole parameters relate to specific impedance properties of the investigated material. The relaxation time τ expresses the scale of the polarization mechanisms, specifically the dominant relaxation period of the polarization. In plant tissues, the polarization originates from the capacitive behavior of the cells due to the polarization of the cell membranes. The relaxation period of this mechanism has been observed in the kHz range. At higher frequencies, the cell membranes only partially polarize because the period of the alternating current is too short to reach the full polarization. Therefore, the cell membranes contribute to the current flow, as a capacitor during its charging, decreasing the electrical impedance. This impedance decrease at high frequencies has been observed with tissue-scale EIS experiments (Bera et al., 2016; Ehosioko et al., 2018; Hayden et al., 1969; Kim et al., 2019; Ozier-Lafontaine & Bajazet, 2005). Repo (1994) interpreted their EIS results on Scots pine (*Pinus*, *Pinus sylvestris*) with a distinction between low-frequency pathways, through vascular tissues and pith intercellular solutions, and high-frequency pathways through intracellular spaces. Because of the similar impedance behavior of the cell membranes, alike impedance response and τ were observed in animal tissues (Teixeira et al., 2018). Nonetheless, some differences are expected, for example, the smaller size of animal cells may lead to shorter relaxation periods (Gabriel et al., 1996).

The Cole–Cole exponent c expresses the distribution of relaxation times. Despite the above main impedance behavior, the complexity of the biological tissues causes

the coexistence of multiple-scale polarization mechanisms, giving rise to a distribution of relaxation time (Zhang et al., 1995). In addition, even when focusing on a single tissue (i.e., homogeneous cells), the distribution of the cell size does not explain the observed dispersion of the relaxation times (Markx et al., 1991). A typical c value for biological tissues is between 0.5 and 0.7 (Kuang & Nelson, 1998; Zhang et al., 1995).

The low-frequency resistance R_0 describes the current conduction when the period of the alternating current is sufficiently long to cause the polarization of the cell membranes. Based on the description of τ , this occurs when the alternating current period is long relative to τ . Then, the polarization of the cell membranes impedes the (displacement) current flow through the symplastic pathway, forcing the current through the apoplastic pathways (Bera, 2018). Meaning, the symplastic pathway has a capacitive behavior, which leads to the frequency dependency of the impedance $Z = 1/i\omega C$. Where Z is the impedance in Ω , i the imaginary unit, ω is the angular frequency in rad s^{-1} , and C is the capacitance F. Because of the hindered conduction through the symplastic pathway, R_0 describes the contribution of the vascular tissues, relating to their physiology and morphology. The low-frequency impedance of plant tissues is typically larger than few $\text{k}\Omega$. Note that R_0 necessarily depends on the geometry of the sample, the above values are typical for laboratory-scale samples (centimeter or few 10s of centimeters). A more precise and comparable analysis would require correcting the impedance value with the geometry of the actual pathways, obtaining their resistivity with the Ohm law. However, the above geometrical correction is rarely performed and challenging because of the variability and complexity of the plant tissues (Hayden et al., 1969; Mary et al., 2017).

The chargeability m is defined from the low-frequency R_0 resistance and the high-frequency resistance R_∞ (Pelton et al., 1978; Seigel, 1959).

$$m = \frac{R_0 - R_\infty}{R_0} \quad (2)$$

As said, the impedance of the biological material tends to decrease with increasing frequency because of the capacitive behavior of the cell membranes (Bera, 2018; Ehosioko et al., 2018). Being proportional to the difference between R_0 and R_∞ , the chargeability quantifies the relevance of this capacitive component of the biological tissue. The chargeability can assume values between 0 and 1 and it is typically higher than 0.5 in biological materials because of their strong capacitive behavior (Cole, 1933; Hayden et al., 1969; Ozier-Lafontaine & Bajazet, 2005).

2.4 | Soil response

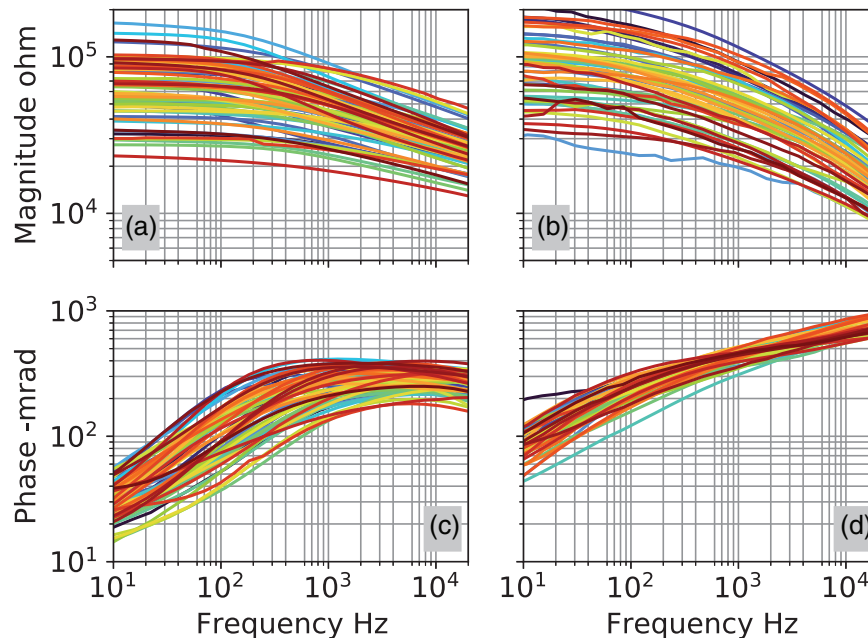
In the context of SRS continuum, it is relevant to review the impedance properties of soil and its similarities with the plant impedance properties. The bulk fluid in the soil pores behaves similarly to the vascular tissue of the plants and provides the major (conduction) current pathways (Kemna et al., 2012). However, soil particles are, in general approximation, considered pure insulators, by contrast to the capacitive behavior of the plant cells (Bücker et al., 2019). Without the intrinsic capacitive behavior of the singular grain, the capacitive response of the soil derives from the impedance properties of the interface between pore fluid and mineral surfaces (Binley et al., 2005; Revil et al., 2015). Consequently, specific surface area and specific surface charge are the key parameters controlling the intensity of the polarization (Peruzzo et al., 2018; Weller & Slater, 2012). Under these conditions, the interfacial polarization in soil is typically significantly smaller than the cell-controlled polarization of biological materials.

In soil, the scale of polarization and, thus, both the characteristic relaxation period and its dispersion relate to the soil texture, in particular to the size of grains and pore. Despite the above differences in the polarization mechanisms, this is similar to dependence of τ and c on the cell size in the plant tissues. Sand and, in first approximation, sandy soil typically have their characteristic polarization frequency at or below few hertz and relatively weak capacitive response (Cassiani et al., 2009; Ulrich & Slater, 2004). On the contrary, clayey soils typically have their characteristic polarization frequency at or above a few 10s of kilohertz, possibly overlapping with the plant response (Leroy & Revil, 2009; Okay et al., 2014). In addition, clayey soils have relative high capacitive response because of their specific surface area and charge. Thus, the soil contribution to the SRS impedance response can be expected to become more significant and harder to decouple with increasing clay content.

2.5 | Cole–Cole fitting

Because of the expected high-frequency polarization of the plant materials and clayey soil, the peak of Cole–Cole term may occasionally lie above the instrumental frequency range. Meaning that only the low-frequency side of the Cole–Cole term is captured. The parameters of these partially-captured Cole–Cole terms may be affected by stronger uncertainty and require regularization. Therefore, constraints for m and τ were included to avoid an unrealistic shift and increase of the Cole–Cole term toward the high frequency. Similar regularization strategy is implemented in Weigand (2017).

FIGURE 2 Magnitude and phase spectra obtained from the root channel in the (a, c) hoop house and (b, d) field acquisitions on wheat plants. Each line represents a plant. Continuous lines are used for the experimental data, rather than dots, because of the large number of spectra. Note that the phase values are shown in negative milliradians (-mrad)



The initial values were derived from the spectra of phase and magnitude. The magnitude value at the lowest frequency (10 Hz) was used as the starting R_0 initial value. The period of the phase peak was used as the starting value for τ . Based on the reviewed literature, both m and c were initially set to 0.5. The fitting routine with regularizations and initial values is publicly available with the code.

2.6 | Direct measurements

Root scanning, soil coring, and shovelomics were used to characterize the root system of the investigated plants. In the field, soil coring was performed the day following the EIS survey. Three cores were collected for each plant with the use of a tractor-mounted hydraulic sampler. The cores measure 8 cm in diameter and 1 m in length. Following the soil coring, the upper 50 cm of the root systems were completely excavated with a shovel (shovelomics). For the hoop house grown plants, the roots were readily extracted from the columns with minimum disturbance thanks to the use of growing bags. After washing, the root systems were scanned (WinRhizo) and analyzed to obtain the average root diameter, total root length, and plant biomass. The roots were then dried to obtain the root dry mass (Freschet et al., 2020).

3 | RESULTS

3.1 | Results from the experiments on the wheat plants

A total of 80 three-channel EIS acquisitions were performed to investigate the wheat plants, 40 in the field and 40 in the

hoop house. Figure 2 shows the EIS magnitude and phase spectra obtained in the hoop house (respectively, a and c) and in the field (respectively, b and d). The figure shows that all the 80 spectra display a significant Cole–Cole frequency dispersion. The impedance values drop in the kilohertz frequency range, while the phase values increase to 100s of milliradians (mrad). This trend is common to all the spectra, but the impedance range over which it occurs varies over an order of magnitude (10s–100s of k Ω). This is highlighted by the Log–Log axes, and indicates a significant variability between field and hoop house data sets, as well as within each of the two data sets. In particular, the magnitude values of the field data sets, compared to the hoop house sets, are higher at low frequency but decrease more quickly and over a wider frequency range.

Figure 3 shows the soil spectra for hoop house and field plants, which was measured with channel 3 in Figure 1. The soil spectra have magnitude values below 10 k Ω and constant over the investigated frequency range. Field magnitudes are larger (few k Ω) than the hoop house values (10s of Ω), reflecting the larger interspace between the potential electrodes (respectively 1 m and 20 cm). The phase values are relatively low (<25 mrad) and constant up to 1 kHz. At higher frequency, the spectra begin to diverge, with some curves increasing with the frequency to maximum values of 75 mrad.

Figure 4 shows the Cole–Cole fitting parameters for the above spectra. The R_0 values, about 100 k Ω , highlight the high impedance magnitude of the plant tissues at low frequency. In line with the spectra, the R_0 values for the field plants are, on average, higher than the hoop house, respectively, 1 and 0.6 k Ω . Similarly, the m values from the field data sets go from 0.9 to 1, while the average value is between 0.7 and 0.8 in the hoop house. The m values reflect the large magnitude

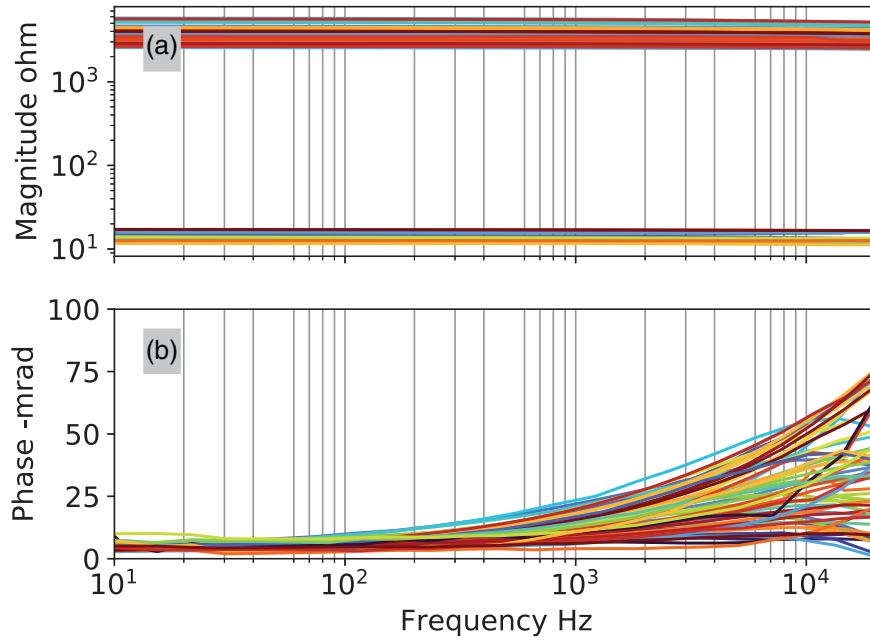


FIGURE 3 (a) Magnitude and (b) phase spectra from the soil channel for both field and hoop house. Note that the phase values are shown in negative milliradians (-mrad)

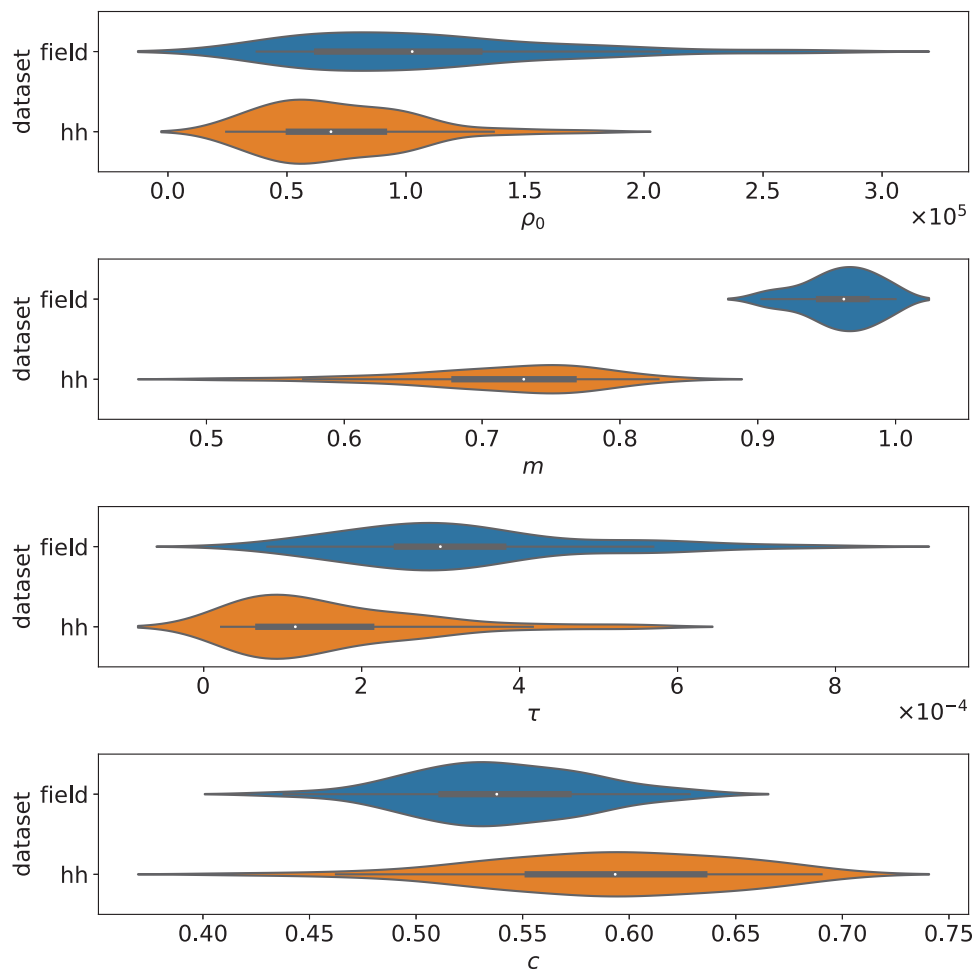


FIGURE 4 Cole-Cole parameters for electrical impedance spectroscopy (EIS) spectra of channel 2, distinguishing between field and hoop house (hh). The full spectra are shown in Figure 2

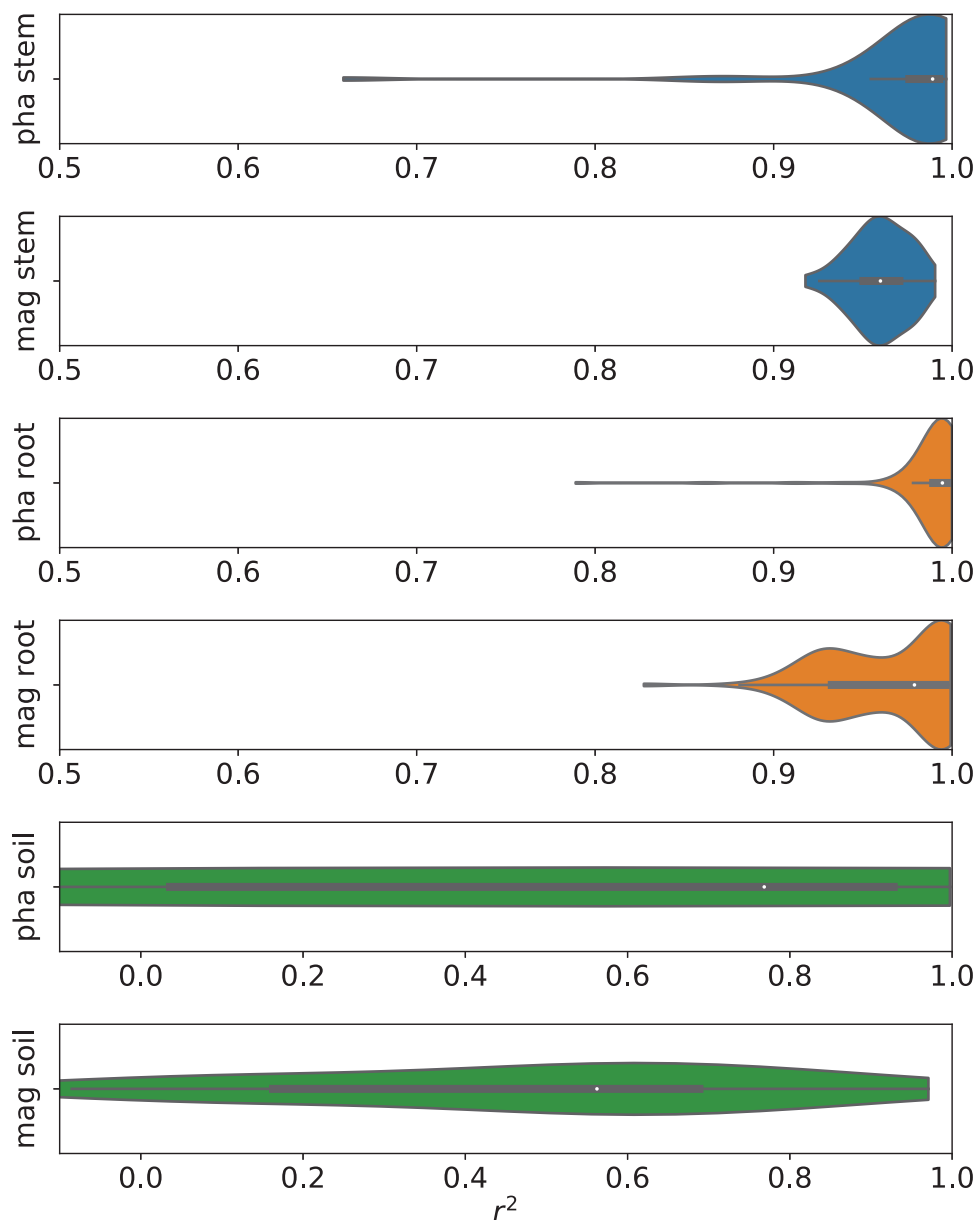


FIGURE 5 Goodness of the Cole–Cole fitting

drop observed in the spectra as the frequency increases. In addition, the m values are also coherent with the larger drop observed in the field spectra relative to the hoop house data (Figure 2). The τ values describe the relatively high frequency polarization observed in the spectra, with relaxation times, on average, between 0.1 and 0.3 ms. Finally, the c values range from 0.4 to 0.75, with mean values between 0.5 and 0.6. These values reflect the wide frequency range of the magnitude drop, particularly in the field spectra.

The goodness of the above Cole–Cole fitting is shown in Figure 5. The single-term Cole–Cole model provides excellent fitting for the channels that are affected by the plant response, that is, stem and root (r^2 values $> .9$). On the contrary, the r^2 values for the soil channel are evenly distributed

between 0 and 1. These low r^2 values reflect the low capacitive response of the soil, which often results in a constant phase value over the spectrum (Figure 3).

Figure 6 highlights the relative unimportance of the soil contribution to the overall SRS impedance response. The figure focuses on the ratios of R_0 and m between the root and soil channels (i.e., $C2/C3$). The ratio values of R_0 indicate that the voltage drop between the two current electrodes, at low frequency, mainly occurs in the plant section. On average, $<5\%$ of the voltage drop occurs in the soil. The value range of m indicates that the capacitive response of the soil is, in average, 10 to 20 times smaller than the plant response.

In contrast to the above ratios, the ratio values in Figure 7 ($C2/C1$) indicate similar impedance properties for the stem

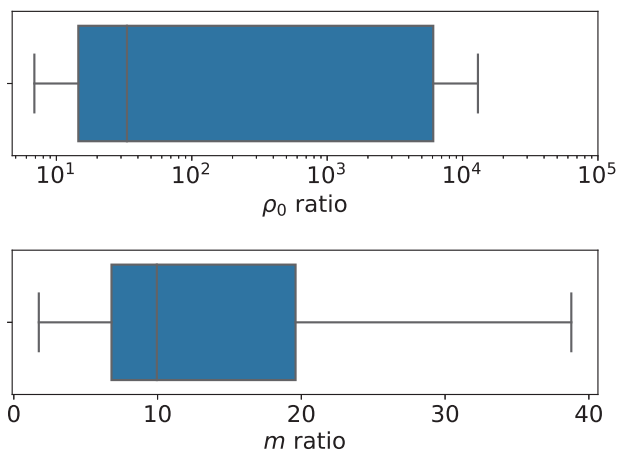


FIGURE 6 Ratio of root channel to soil channel for R_0 and m

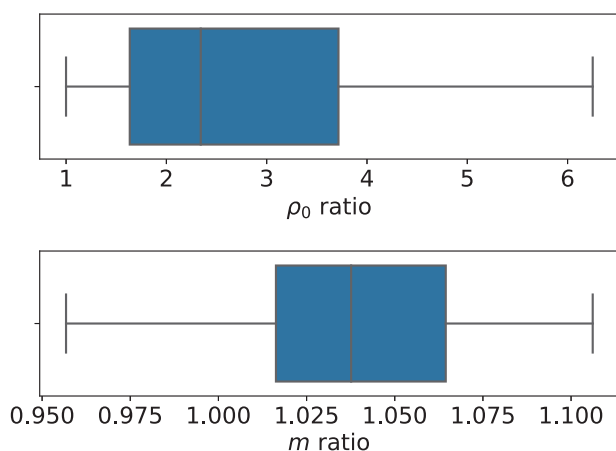


FIGURE 7 Ratio of root channel to stem channel for R_0 and m

and root sections. In particular, the values of the chargeability m ratios are close to the unity, on average between 1.025 and 1.05. With regard to the low frequency response, the potential drop is similarly distributed between the stem and the roots, with R_0 ratios in average between 2 and 3. Note that, because of the overlap between C1 and C2 channels, the stem drop also contributes to the root channel response (Figure 1).

In addition to the EIS acquisitions, direct plant measurements were performed. Figure 8 shows the results of these direct measurements, including the most common root traits (length, weight, and average diameter) and shoot biomass. The figure distinguishes between field and hoop house plants, highlighting the higher values of root length, root weight, and shoot biomass for the field plants. This is coherent with the direct observation of the two sets of wheat plants during the experiments, when the field plants were visibly bigger than the hoop house plants. On the contrary, the values of average root diameter are very similar between field on hoop house, with both mean values between 0.4 and 0.5 mm. Figure 9 further focuses on these correlations between shoot biomass and

root traits. Both root length and root weight appear strongly correlated with the shoot biomass, in both field and hoop house datasets. Despite the similar distribution of the average diameter in Figure 9, the values of the field dataset present a certain degree of dependency on the shoot mass, which is not observed in the hoop house data.

Figure 10 combines the EIS results, in terms of Cole–Cole parameters, and the direct measurements of shoot biomass and root traits. Among the Cole–Cole parameters, the chargeability m resulted the more interesting in terms of sensitivity to the above plant variables. The figure shows a good correlation between m and the root length ($.73 r^2$ with an exponential model). At the same time, a similar trend is visible between shoot biomass and root length ($.54 r^2$). The figure also highlights how the data points of each cultivar tend to cluster. The overall trend mainly results from an alignment of these clusters rather than intra-cultivar correlation. The only exception is the cultivar TAM111, whose data are common to both field and hoop house and better align with the general trend.

The result of the 20 acquisitions exploring the intra-plant (i.e., among the tillers of a plant) variability indicates that the EIS response change among the tillers of the same plants. However, the intra-plant variability is statistically lower than the inter-plant variability observed among tillers of different plants in the field, see Figure 4. The percentage variability of the chargeability m is lower than 7%, 25% for τ , 10% for R_0 , and 7% for c .

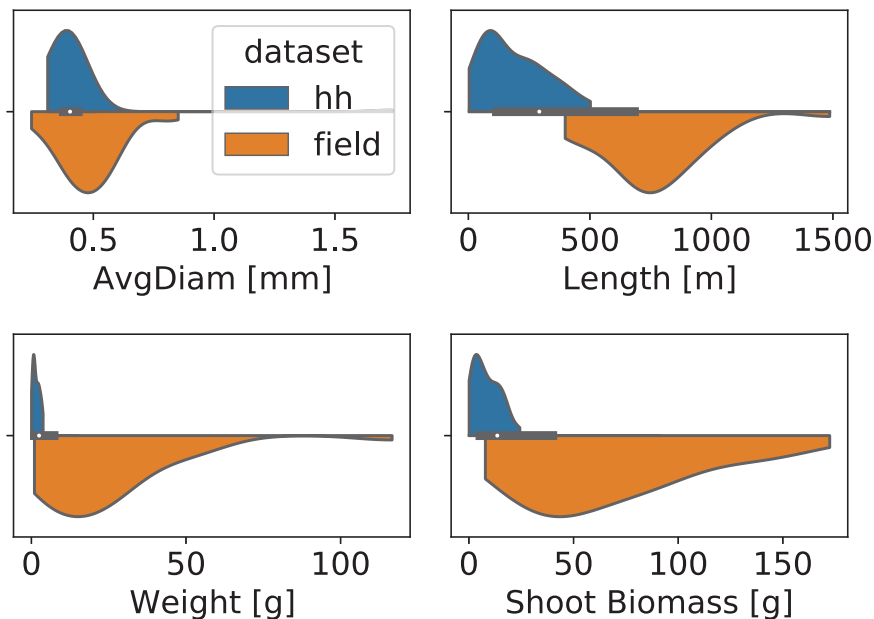
3.2 | Results from the experiments on the pecan plants

We performed the EIS acquisitions on the 10 pecan plants following the column configuration used for wheat plants in the hoop house plants (Figure 1). Figure 11 shows the EIS acquired spectra. Similarly to the wheat results, the spectra show high magnitude values at low frequency and a pronounced capacitive behavior, which leads to a significant magnitude drop in the kilohertz frequency range. This also leads to high phase peak values, which range between 0.2 and 0.6 rad. Because of the limited number of datasets, the figure displays both the raw data (dots) and the fitted Cole–Cole models (lines). This highlights that the Cole–Cole model provides an excellent fitting of the pecan data, with an r^2 of .96.

4 | DISCUSSION

We reviewed how researchers in plant sciences have long been exploring the use of electrical methods for noninvasive root studies. Among the tested electrical methods, the EIS is the most comprehensive and, thus, suited to capture the information-rich impedance response of plants and other

FIGURE 8 Distribution of main measured root traits and shoot biomass for field and hoop house (hh) plants



biological materials. However, despite the numerous attempts and the known EIS sensitivity to the biological properties, a few aspects have hindered the upscaling of the EIS to field applications. It was highlighted how the understanding of the current pathways in the SRS continuum is a key point for the correct interpretation of the EIS results. Finally, we motivated that the EIS spectra require some parameterization in order to be better included in the statistical analysis of root phenotyping and selection. This study addresses the above issues with a combination of three-channel EIS setup and Cole–Cole fitting of the resulting spectra, providing the first large-scale EIS application to root phenotyping.

The measured SRS spectra show a strong capacitive response, with high values of magnitude that decrease in the 10s of kilohertz frequency range. This EIS response is common to all the plants, providing the first extensive and field confirmation of recent EIS laboratory studies (Ehosioko et al., 2018; Kim et al., 2019; Mary et al., 2017). The observed impedance response is attributed to the capacitive behavior of the plant cells, in line with the studies that suggest the coexistence of a low-frequency intercellular (apoplastic) pathway and high-frequency intracellular (symplastic) pathway (Bera et al., 2016; Bera, 2018; Jócsák et al., 2019). Our extensive EIS investigation indicates that this transition between the two pathways occurs in the kilohertz frequency range.

In contrast to the plant response, the soil EIS spectra present significantly lower magnitude and phase values (Figure 3). This soil response is in line with the reviewed literature and soil polarization mechanisms (Bücker et al., 2019; Kemna et al., 2012). The difference between field and hoop house magnitude values is caused by the larger interspace of the field soil electrodes and simply reflects the sensitivity of the EIS signals to the electrode geometry. While the clayey soil

may explain the increasing phase values at high frequency, the particular divergence of the trends suggests the presence of instrumental errors. In addition, the expectancy of instrumental errors in the soil spectra increases because of the significantly lower capacitive response with respect to the plant channels (C1 and C2). The PSIP adjustment for the high capacitive responses of the plant tissues makes the measurement of the soil channel more susceptible to instrumental noise, which commonly manifests as the frequency increases (Abdulsamad et al., 2016).

The single-term Cole–Cole model well describes the characteristic impedance response of the investigated plants (Figure 5). The Cole–Cole fitting provides convenient parameters that capture and summarize the information-rich EIS spectra, allowing their quantitative and statistical analysis. The analysis of the τ values summarizes the presence and variability of the dominant polarization in the 10s kilohertz frequency range. This is in line with the raw spectra (Figures 2 and 4), and quantitatively locates the transition frequency range between apoplastic and symplastic pathways. The c values agree with the reviewed literature and capture the width of the frequency range over which the above transition occurs (Kuang & Nelson, 1998; Zhang et al., 1995). Finally, the values of R_0 and m quantify the strong capacitive behavior of the plant tissues and its variations between the different plants, particularly between field and hoop house plants (Figures 4 and 5).

The Cole–Cole fitting also allows the comparison of the three EIS channels. Comparing plant and soil responses, the ratio values for m and R_0 indicate that plant tissues dominate both in terms of low-frequency impedance and capacitive response. Interestingly, this negligible soil contribution is observed for all plants, despite the clayey growing medium

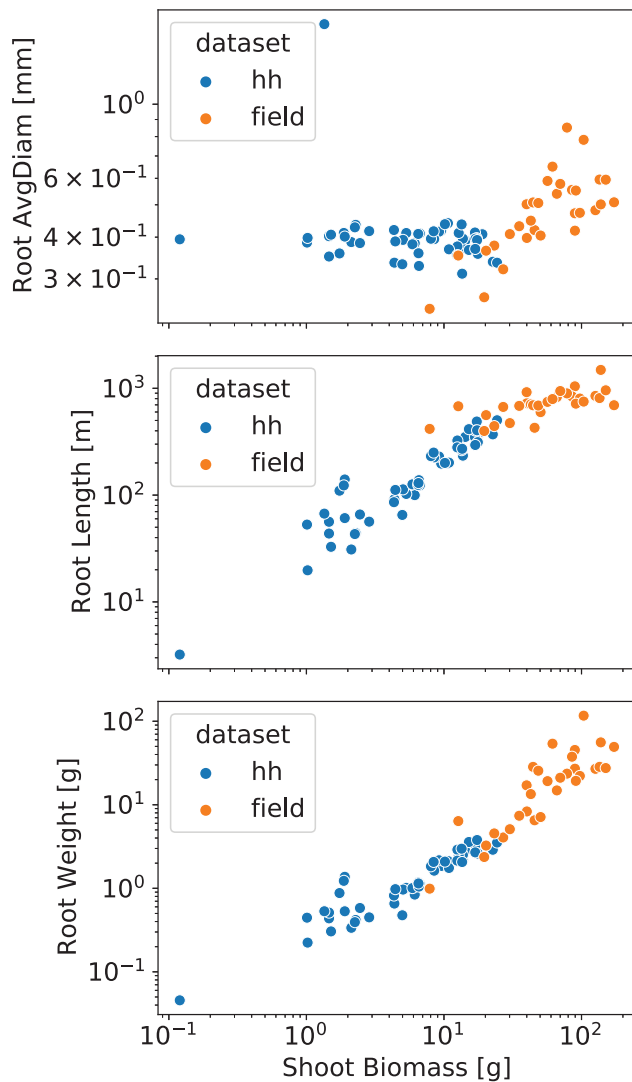


FIGURE 9 Correlations between root traits and shoot biomass for field and hoop house (hh) plants

and relatively long length of soil channel compared to the stem and root channels. Therefore, the dominant effect of the plant response can be expected to be a general condition. This result shows how the analysis of the soil channel successfully addresses and reduces the concern on the soil impact on the EIS investigation (Hermanská et al., 2015; Urban et al., 2011). A similar conclusion was reached by Cseresnyés et al. (2013).

On the contrary, the comparison of the stem and root channels shows that the stem section significantly contributes to the overall response of the SRS system (Figure 7). The similar m and τ values between stem and root channels suggest that the additional current path in the roots, after the stem section, has similar impedance properties. This similar response supports, to some degree, a possible homogeneity assumption between the stem and investigated part of the root system in terms of impedance properties. In particular, the transition between symplastic and apoplasmic pathways is the dominant

EIS factor for both stem and investigated part of the root system. With regard to the extent of the investigated part of the root system, the ratio values of R_0 indicate that resistance of the current pathways measured by C2 is few (two to three) times the stem resistance measured by C1. Then, the homogeneity assumption of the root system suggests that the current pathways in the plant extend from the stem section proportionally to these increment percentages, which is only a few centimeters (Figure 7). This reasoning on the current pathways extent is also supported by the relative low values of R_0 for the soil channel. Meaning that, despite the longer current path in the soil, particularly in the field, the impedance of the soil channel is on average 10 times smaller. Consequently, the current flow is expected to prefer the less-resistive soil pathways (i.e., path of least resistance). This agrees with the possibility for proximal current leakage discussed in Urban et al. (2011) and Dietrich et al. (2012). In the specific of this study on wheat plants, the ratio values between 2 and 3 agree with recent imaging investigation of the SRS current pathways of crop plants (Peruzzo et al., 2020).

The direct measurements on plants and roots support the interpretation of the EIS results. Because of the different cultivars and growing conditions, there is a significant variability in both shoot biomass and root traits, particularly between field and hoop house plants. The higher values of biomass of the field plants are likely related to the unconstrained root growth compared to the column plants in the hoop house. The same is observed for the main measured root traits, which results in a significant correlation between shoot biomass and root length and weight (Figure 9). On the contrary the average diameter of the roots appears uncorrelated with the shoot biomass for the hoop house plants and weakly correlated for the field plants.

A more comprehensive interpretation of the EIS results is possible considering both the root traits (Figure 8) and their correlations with the shoot biomass (Figure 9), as well as the above discussion on the relationship between the EIS channels (Figures 6 and 7). On the one hand, the correlations between the root traits and the EIS signals support the research and application of noninvasive EIS phenotyping solutions, that is, the use of electrical proxies for environmentally relevant root traits (Dietrich et al., 2012; Jócsák et al., 2019; Postic & Doussan, 2016). In our study, we highlight that the Cole–Cole chargeability m shows a good and promising correlation with the root length of wheat and pecan plants (Figures 10 and 12), a key environmental root trait (Jócsák et al., 2019). In this sense, our study agrees and upscales previous lab-scale investigations on crop plants, see Dietrich et al. (2012), their Table 1; Postic and Doussan (2016), their Table 3; and Jócsák et al. (2019). On the other hand, the correlations between root traits and shoot biomass become crucial when considering the dominant contribution of the stem response to the overall SRS response and the above indications for proximal current

FIGURE 10 Correlations between the Cole–Cole chargeability m and (a) root length and (b) shoot biomass

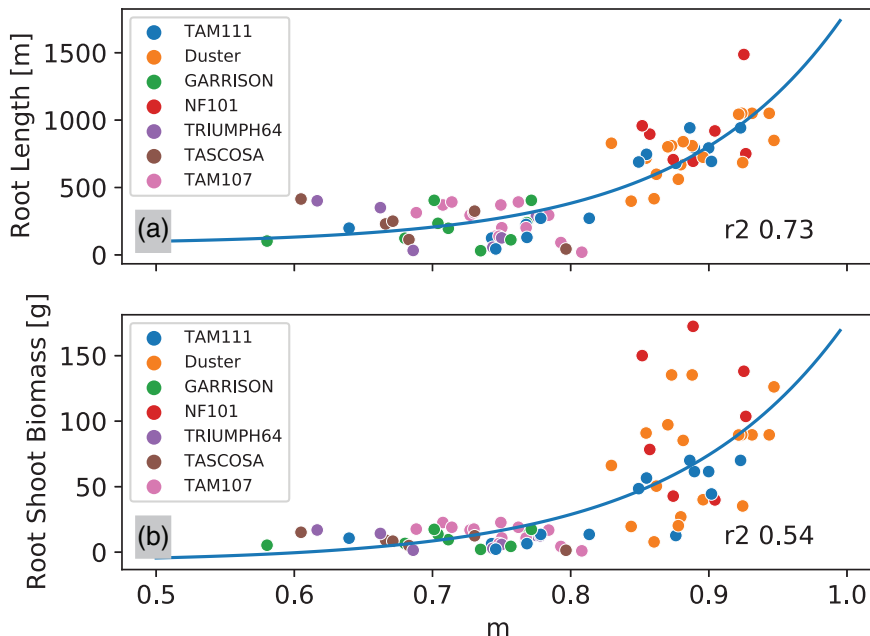
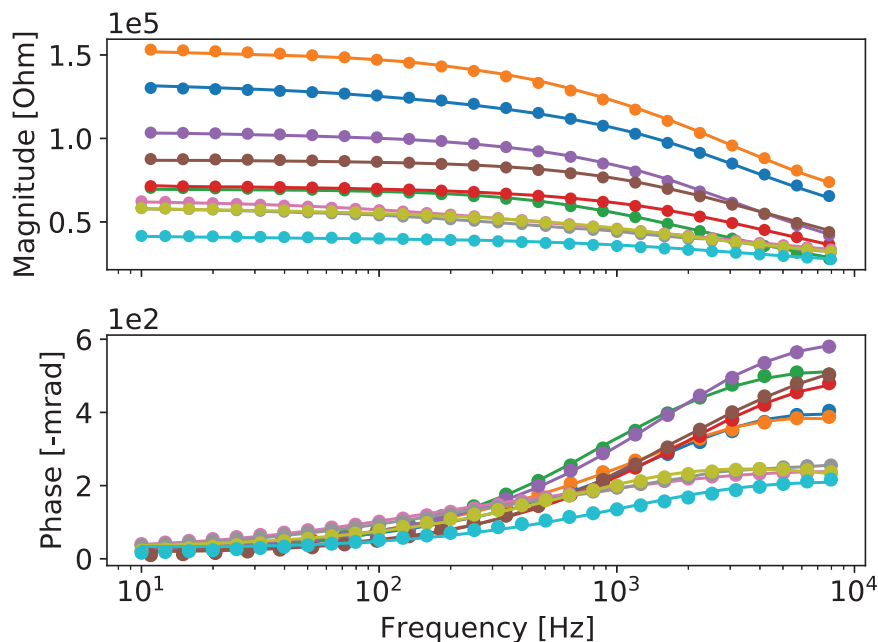


FIGURE 11 Magnitude and phase spectra of the root channel of the pecan plants, together with their Cole–Cole fitting. Dots are the measured values and continuous lines are the fitted Cole–Cole models. The average r^2 for the Cole–Cole fitting on pecan plants is 0.96



leakage. The proximal current leakage implies that the distal part of the root system has little impact on the EIS signal. This interpretation supports the growing concern on the meaning of the EIS signals, reviewed in the introduction. However, the experimental evidence supporting the EIS sensitivity and correlations with root traits indicates that the EIS method can predict root properties despite the possible current leakage, for example, Figure 10, and references in Dietrich et al. (2012), Postic and Doussan (2016), Jócsák et al. (2019). Note also how the research of EIS-roots correlations typically targets physiologically relevant root traits which strongly depend on the distal parts of the root system, such as root-absorbing area and root length. In regard to this open issue and apparent con-

tradition, our study provides the first large-scale evidence for proximal current leakage and highlights the key role of the correlations between root traits and properties of the aerial and/or proximal part of the root system. In our study, stem and proximal part of the root system control the EIS response of the SRS system, and their physiological correlations with the root traits lead to the correlation between EIS signal and root length, which is then to be considered an indirect correlation.

The intra-plant variability observed among tillers of a same plant implies that the EIS response depends on the number of tillers and their interconnection. Few studies have shown how wheat tillers develop an increasing degree of nutritional autonomy during the plant growth (Day & Atkin, 1985;

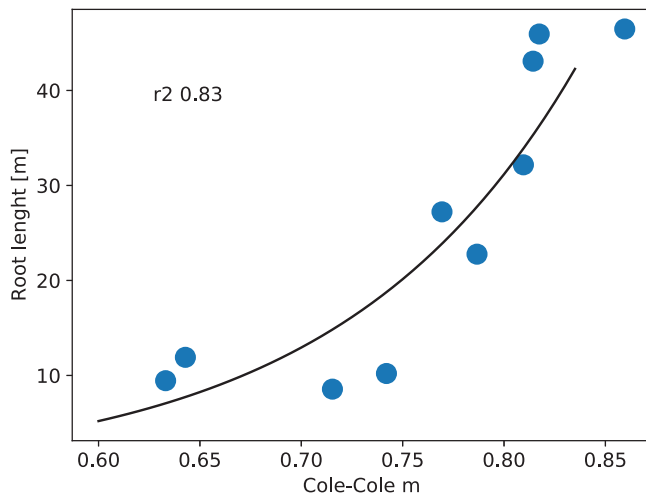


FIGURE 12 Correlation between the chargeability m and the root length for the pecan plants

Hendriks et al., 2016; Quinlan & Sagar, 1962; Rickman et al., 1985). The root system would be to some extent divided among tillers and/or groups of connected tillers, in particular because of the presence of adventitious roots and secondary tillers. Only the part of the root system associated with the investigated tiller would contribute to the EIS response. In this sense, we measured the number of tillers of each plant and used it to “normalize” the measured root traits (dividing the root trait by the number of tillers). The correlation between EIS response and the obtained normalized root traits improved to .78 r^2 for the root length. The higher value observed for pecan plants, .83 r^2 , may also reflect and benefit from the absence of the complex tillering physiological implications. However, based on the same differences between tillers of the same plant, we highlight how dividing evenly by the number of tillers is simply an exploratory and qualitative solution. While this study explored the tillering influence, supporting its relevance and showing the EIS potential in this regard, an exhaustive investigation is beyond the present scope and would necessarily require more detailed physiological investigations.

5 | CONCLUSIONS

We reviewed the extensive EIS research effort for noninvasive root investigation, and highlighted how the methodological limitations lead to contradictions and hindered the upscaling to field scale. We proposed a combination of three-channel acquisitions and Cole–Cole fitting to specifically target and quantitatively analyze the EIS root signals within the SRS response. The proposed solutions provided: (a) insight on the key contribution of the plant stem to the overall SRS response;

(b) knowledge on the differences and relative importance of plant and soil EIS signals; (c) evidence supporting the concerns on the proximal current leakage in herbaceous roots; (d) statistical corroboration for the use of the Cole–Cole model as a way to conveniently capture and summarize the EIS spectra; (e) a novel framework for the correct interpretation of the observed correlations between EIS signals and root traits, to advance and upscale the use of EIS in field root phenotyping. While confirming the sensitivity of the EIS signals to relevant physiological variables, which we recognized in the indirect correlations with the root traits, this study defines methodological possibilities and limitations, as well as general practices to better address these limitations in laboratory experiments and field applications. Future studies are needed on different root types, particularly on woody roots where deeper current penetration pathways have been observed. This future work may also benefit from a more extensive physiological characterization of the root system and its connection with the plant stem, as highlighted by the intra-plant variability results.

ACKNOWLEDGMENTS

The authors acknowledge the support of ARPA-E ROOTS (Advanced Research Projects Agency - Energy, Rhizosphere Observations Optimizing Terrestrial Sequestration, Lawrence Berkeley National Laboratory). Benjamin Mary acknowledges the financial support from European Union’s Horizon 2020 research and innovation programme under a Marie Skłodowska-Curie grant agreement (grant no. 842922). Maximilian Weigand was partially funded by the Deutsche Forschungsgemeinschaft (DFG, German Research Foundation) under Germany’s Excellence Strategy – EXC 2070 – 390732324. Luca Peruzzo thanks Irene Tonelato for illustrating Figure 1.

AUTHOR CONTRIBUTIONS

Luca Peruzzo: Conceptualization; Investigation; Methodology; Writing-original draft; Writing-review & editing. Liu Xiuwei: Conceptualization; Investigation; Methodology; Writing-original draft. Chunwei Chou: Conceptualization; Investigation; Methodology. Alison B. Blancaflor: Conceptualization; Supervision. Haijun Zhao: Conceptualization; Investigation. Xue-Feng Ma: Investigation; Resources. Benjamin Mary: Data curation; Investigation; Methodology; Writing-review & editing. Maximilian Weigand: Conceptualization; Methodology; Writing-review & editing. Veronika Iván: Investigation; Writing-review & editing. Yuxin Wu: Conceptualization; Funding acquisition; Supervision; Writing-review & editing

CONFLICT OF INTEREST

The authors declare no conflict of interest.

ORCID

Luca Peruzzo  <https://orcid.org/0000-0002-4065-8910>

Xue-Feng Ma  <https://orcid.org/0000-0002-0942-9116>

Benjamin Mary  <https://orcid.org/0000-0001-7199-2885>

REFERENCES

- Abdulsamad, F., Florsch, N., Schmutz, M., & Camerlynck, C. (2016). Assessing the high frequency behavior of non-polarizable electrodes for spectral induced polarization measurements. *Journal of Applied Geophysics*, 135, 449–455. <https://doi.org/10.1016/j.jappgeo.2016.01.001>
- Atkinson, J. A., Pound, M. P., Bennett, M. J., & Wells, D. M. (2019). Uncovering the hidden half of plants using new advances in root phenotyping. *Current Opinion in Biotechnology*, 55, 1–8. <https://doi.org/10.1016/j.copbio.2018.06.002>
- Aubrecht, L., Stanek, Z., & Koller, J. (2006). Electrical measurement of the absorption surfaces of tree roots by the earth impedance method: 1. Theory. *Tree Physiology*, 26(9), 1105–1112. <https://doi.org/10.1093/treephys/26.9.1105>
- Bera, T. K. (2014). Bioelectrical impedance methods for noninvasive health monitoring: A review. *Journal of Medical Engineering*, 2014, 1–28. <https://doi.org/10.1155/2014/381251>
- Bera, T. K. (2018). Bioelectrical impedance and the frequency dependent current conduction through biological tissues: A short review. *IOP Conference Series: Materials Science and Engineering*, 331, 012005. <https://doi.org/10.1088/1757-899X/331/1/012005>
- Bera, T. K., Nagaraju, J., & Lubineau, G. (2016). Electrical impedance spectroscopy (EIS)-based evaluation of biological tissue phantoms to study multifrequency electrical impedance tomography (MF-EIT) systems. *Journal of Visualization*, 19(4), 691–713. <https://doi.org/10.1007/s12650-016-0351-0>
- Binley, A., & Kemna, A. (2005). DC resistivity and induced polarization methods. In Y. Rubin & S. S. Hubbard (Eds.), *Hydrogeophysics* (Volume 50, pp. 129–156). Dordrecht: Springer Netherlands.
- Binley, A., Slater, L. D., Fukes, M., & Cassiani, G. (2005). Relationship between spectral induced polarization and hydraulic properties of saturated and unsaturated sandstone: Sandstone SIP-hydraulic relationships. *Water Resources Research*, 41(12). <https://doi.org/10.1029/2005WR004202>
- Bücker, M., Flores Orozco, A., Undorf, S., & Kemna, A. (2019). On the role of Stern- and diffuse-layer polarization mechanisms in porous media. *Journal of Geophysical Research: Solid Earth*, 124(6), 5656–5677.
- Butler, T. J., Biermacher, J. T., Kering, M. K., & Interrante, S. M. (2012). Production and economics of grazing steers on rye-annual ryegrass with legumes or fertilized with nitrogen. *Crop Science*, 52(4), 1931–1939. <https://doi.org/10.2135/cropsci2011.11.0611>
- Cao, Y., Repo, T., Silvennoinen, R., Lehto, T., & Pelkonen, P. (2010). An appraisal of the electrical resistance method for assessing root surface area. *Journal of Experimental Botany*, 61(9), 2491–2497. <https://doi.org/10.1093/jxb/erq078>
- Cassiani, G., Boaga, J., Vanella, D., Perri, M. T., & Consoli, S. (2015). Monitoring and modelling of soil-plant interactions: The joint use of ERT, sap flow and eddy covariance data to characterize the volume of an orange tree root zone. *Hydrology and Earth System Sciences*, 19(5), 2213–2225. <https://doi.org/10.5194/hess-19-2213-2015>
- Cassiani, G., Kemna, A., Villa, A., & Zimmermann, E. (2009). Spectral induced polarization for the characterization of free-phase hydrocarbon contamination of sediments with low clay content. *Near Surface Geophysics*, 7(5-6), 547–562. <https://doi.org/10.3997/1873-0604.2009028>
- Čermák, J., Cudlín, P., Gebauer, R., Börja, I., Martinková, M., Staněk, Z., Koller, J., Neruda, J., & Nadezhdina, N. (2013). Estimating the absorptive root area in Norway spruce by using the common direct and indirect earth impedance methods. *Plant and Soil*, 372(1-2), 401–415. <https://doi.org/10.1007/s11104-013-1740-y>
- Cermak, J., Ulrich, R., Stanek, Z., Koller, J., & Aubrecht, L. (2006). Electrical measurement of tree root absorbing surfaces by the earth impedance method: 2. Verification based on allometric relationships and root severing experiments. *Tree Physiology*, 26(9), 1113–1121. <https://doi.org/10.1093/treephys/26.9.1113>
- Cole, K. S. (1933). Electric conductance of biological systems. *Cold Spring Harbor Symposia on Quantitative Biology*, 1(0), 107–116. <https://doi.org/10.1101/SQB.1933.001.01.014>
- Cseresnyés, I., Rajkai, K., & Vozáry, E. (2013). Role of phase angle measurement in electrical impedance spectroscopy. *International Agro-physiology*, 27(4), 377–383. <https://doi.org/10.2478/intag-2013-0007>
- Cseresnyés, I., Vozáry, E., & Rajkai, K. (2020). Does electrical capacitance represent roots in the soil? *Acta Physiologiae Plantarum*, 42(5), 71. <https://doi.org/10.1007/s11738-020-03061-9>
- Dalton, F. N. (1995). In-situ root extent measurements by electrical capacitance methods. *Plant and Soil*, 173(1), 157–165. <https://doi.org/10.1007/BF00155527>
- Day, W., & Atkin, R. K. E. (1985). *Wheat growth and modelling*. Boston, MA: Springer US.
- Dietrich, R. C., Bengough, A. G., Jones, H. G., & White, P. J. (2012). A new physical interpretation of plant root capacitance. *Journal of Experimental Botany*, 63(17), 6149–6159. <https://doi.org/10.1093/jxb/ers264>
- Ehosioke, S., Garre, S., Kremer, T., Rao, S., Kemna, A., Huisman, J. A., Zimmermann, E., Javaux, M., & Nguyen, F. (2018). A new method for characterizing the complex electrical properties of root segments. In ISSR International Symposium: Israel: Exposing the hidden half. 10(1–10). Israel, Ma'ale HaHamisha: International Society of Root Researchers (ISRR).
- Ehosioke, S., Nguyen, F., Rao, S., Kremer, T., Placencia-Gomez, E., Huisman, J. A., Kemna, A., Javaux, M., & Garré, S. (2020). Sensing the electrical properties of roots: A review. *Vadose Zone Journal*, 19(1), 1–29. <https://doi.org/10.1002/vzj2.20082>
- Enstone, D. E., & Peterson, C. A. (2005). Suberin lamella development in maize seedling roots grown in aerated and stagnant conditions. *Plant, Cell and Environment*, 28(4), 444–455. <https://doi.org/10.1111/j.1365-3040.2005.01286.x>
- Freschet, G. T., Pagès, L. L., Iversen, C., Comas, L. H., Rewald, B., Roumet, C., Klimešová, J., Zadworny, M., Poorter, H., Postma, J. A., Adams, T. S., Bagniewska-Zadworna, A., Bengough, A. G., Blancaflor, E. B., Brunner, I., Cornelissen, J. H. C., Garnier, E., Gessler, A., Hobbie, S. E., ... McCormack, M. L. (2020). *A starting guide to root ecology: Strengthening ecological concepts and standardizing root classification, sampling, processing and trait measurements*. hal-02918834.
- Gabriel, C., Gabriel, S., & Corthout, E. (1996). The dielectric properties of biological tissues: I. Literature survey. *Physics in Medicine and Biology*, 41(11), 2231–2249. <https://doi.org/10.1088/0031-9155/41/11/001>
- Hayden, R. I., Moyle, C. A., Calder, F. W., Crawford, D. P., & Fensom, D. S. (1969). Electrical impedance studies on potato and alfalfa tissue.

- Journal of Experimental Botany*, 20(2), 177–200. <https://doi.org/10.1093/jxb/20.2.177>
- Hendriks, P. W., Kirkegaard, J. A., Lilley, J. M., Gregory, P. J., & Rebetzke, G. J. (2016). A tillering inhibition gene influences root-shoot carbon partitioning and pattern of water use to improve wheat productivity in rainfed environments. *Journal of Experimental Botany*, 67(1), 327–340. <https://doi.org/10.1093/jxb/erv457>
- Heřmanská, A., Středa, T., & Chloupek, O. (2015). Improved wheat grain yield by a new method of root selection. *Agronomy for Sustainable Development*, 35(1), 195–202. <https://doi.org/10.1007/s13593-014-0227-4>
- Jaffrin, M. Y., & Morel, H. (2008). Body fluid volumes measurements by impedance: A review of bioimpedance spectroscopy (BIS) and bioimpedance analysis (BIA) methods. *Medical Engineering & Physics*, 30(10), 1257–1269.
- Jócsák, I., Végvári, G., & Vozáry, E. (2019). Electrical impedance measurement on plants: A review with some insights to other fields. *Theoretical and Experimental Plant Physiology*, 31(3), 359–375. <https://doi.org/10.1007/s40626-019-00152-y>
- Kemna, A., Binley, A., Cassiani, G., Niederleithinger, E., Revil, A., Slater, L., Williams, K. H., Orozco, A. F., Haegel, F. - H., Hördt, A., Kruschwitz, S., Leroux, V., Titov, K., & Zimmermann, E. (2012). An overview of the spectral induced polarization method for near-surface applications. *Near Surface Geophysics*, 10(6), 453–468. <https://doi.org/10.3997/1873-0604.2012027>
- Kim, J. J., Allison, L. K., & Andrew, T. L. (2019). Vapor-printed polymer electrodes for long-term, on-demand health monitoring. *Science Advances*, 5(3), eaaw0463. <https://doi.org/10.1126/sciadv.aaw0463>
- Kuang, W. & Nelson, S. O. (1998). Low-frequency dielectric properties of biological tissues: A review with some new insights. *Transactions of the ASAE*, 41(1), 173–184. <https://doi.org/10.13031/2013.17142>
- Leroy, P., & Revil, A. (2009). A mechanistic model for the spectral induced polarization of clay materials. *Journal of Geophysical Research*, 114(B10), B10202. <https://doi.org/10.1029/2008JB006114>
- Macnae, J. (2015). Comment on: Tarasov, A. & Titov, K., 2013, On the use of the Cole-Cole equations in spectral induced polarization. *Geophys. J. Int.*, 195, 352–356. *Geophysical Journal International*, 202(1), 529–532. <https://doi.org/10.1093/gji/ggv131>
- S. Mancuso (Ed.). (2012). *Measuring roots: An updated approach*. *Life sciences*. New York: Springer.
- Markx, G. H., Davey, C. L., & Kell, D. B. (1991). To what extent is the magnitude of the Cole-Cole α of the β -dielectric dispersion of cell suspensions explicable in terms of the cell size distribution? *Journal of Electroanalytical Chemistry and Interfacial Electrochemistry*, 320(2), 195–211. [https://doi.org/10.1016/0022-0728\(91\)85627-2](https://doi.org/10.1016/0022-0728(91)85627-2)
- Mary, B., Abdulsamad, F., Saracco, G., Peyras, L., Vennetier, M., Mériaux, P., & Camerlynck, C. (2017). Improvement of coarse root detection using time and frequency induced polarization: From laboratory to field experiments. *Plant and Soil*, 417(1-2), 243–259. <https://doi.org/10.1007/s11104-017-3255-4>
- Mary, B., Peruzzo, L., Boaga, J., Cenni, N., Schmutz, M., Wu, Y., Hubbard, S. S., & Cassiani, G. (2020). Time-lapse monitoring of root water uptake using electrical resistivity tomography and mise-à-la-masse: A vineyard infiltration experiment. *Soil*, 6(1), 95–114. <https://doi.org/10.5194/soil-6-95-2020>
- Mary, B., Peruzzo, L., Boaga, J., Schmutz, M., Wu, Y., Hubbard, S. S., & Cassiani, G. (2018). Small-scale characterization of vine plant root water uptake via 3-D electrical resistivity tomography and mise-à-la-masse method. *Hydrology and Earth System Sciences*, 22(10), 5427–5444. <https://doi.org/10.5194/hess-22-5427-2018>
- Mary, B., Vanella, D., Consoli, S., & Cassiani, G. (2019). Assessing the extent of citrus trees root apparatus under deficit irrigation via multi-method geo-electrical imaging. *Scientific Reports*, 9(1), 9913. <https://doi.org/10.1038/s41598-019-46107-w>
- Mcbride, R., Candido, M., & Ferguson, J. (2008). Estimating root mass in maize genotypes using the electrical capacitance method. *Archives of Agronomy and Soil Science*, 54(2), 215–226. <https://doi.org/10.1080/03650340701790658>
- Okay, G., Leroy, P., Ghorbani, A., Cosenza, P., Camerlynck, C., Cabrera, J., Florsch, N., & Revil, A. (2014). Spectral induced polarization of clay-sand mixtures: Experiments and modeling. *Geophysics*, 79(6), E353–E375. <https://doi.org/10.1190/geo2013-0347.1>
- Ozier-Lafontaine, H., & Bajazet, T. (2005). Analysis of root growth by impedance spectroscopy (EIS). *Plant and Soil*, 277(1-2), 299–313. <https://doi.org/10.1007/s11104-005-7531-3>
- Pelton, W. H., Ward, S. H., Hallof, P. G., Sill, W. R., & Nelson, P. H. (1978). Mineral discrimination and removal of inductive coupling with multifrequency ip. *Geophysics*, 43(3), 588–609. <https://doi.org/10.1190/1.1440839>
- Peruzzo, L., Chou, C., Wu, Y., Schmutz, M., Mary, B., Wagner, F. M., Petrov, P., Newman, G., Blancaflor, E. B., Liu, X., Ma, X., & Hubbard, S. (2020). Imaging of plant current pathways for non-invasive root Phenotyping using a newly developed electrical current source density approach. *Plant and Soil*, 450(1-2), 567–584. <https://doi.org/10.1007/s11104-020-04529-w>
- Peruzzo, L., Schmutz, M., Franceschi, M., Wu, Y., & Hubbard, S. S. (2018). The relative importance of saturated silica sand interfacial and pore fluid geochemistry on the spectral induced polarization response. *Journal of Geophysical Research: Biogeosciences*, 123(5), 1702–1718.
- Postic, F., & Doussan, C. (2016). Benchmarking electrical methods for rapid estimation of root biomass. *Plant Methods*, 12(1), 33. <https://doi.org/10.1186/s13007-016-0133-7>
- Quinlan, J. D., & Sagar, G. R. (1962). An autoradiographic study of the movement of ¹⁴C-labelled assimilates in the developing wheat plant. *Weed Research*, 2(4), 264–273. <https://doi.org/10.1111/j.1365-3180.1962.tb00209.x>
- Redjala, T., Zelko, I., Sterckeman, T., Legué, V., & Lux, A. (2011). Relationship between root structure and root cadmium uptake in maize. *Environmental and Experimental Botany*, 71(2), 241–248. <https://doi.org/10.1016/j.envexpbot.2010.12.010>
- Repo, T. (1994). Influence of different electrodes and tissues on the impedance spectra of Scots pine shoots. *Electro- and Magnetobiology*, 13(1), 1–14. <https://doi.org/10.3109/15368379409030694>
- Repo, T., Laukkanen, J., & Silvennoinen, R. (2005). Measurement of the tree root growth using electrical impedance spectroscopy. *Silva Fennica*, 39(2). <https://doi.org/10.14214/sf.380>
- Revil, A., Binley, A., Mejus, L., & Kessouri, P. (2015). Predicting permeability from the characteristic relaxation time and intrinsic formation factor of complex conductivity spectra: Permeability from spectral induced polarization spectra. *Water Resources Research*, 51(8), 6672–6700. <https://doi.org/10.1002/2015WR017074>
- Rickman, R. W., Klepper, B., & Belford, R. K. (1985). Developmental relationships among roots, leaves and tillers in winter wheat. In W. Day & R. K. Atkin (Eds.), *Wheat growth and modelling* (pp. 83–98). Boston, MA: Springer US.

- Rücker, C., Günther, T., & Wagner, F. M. (2017). pyGIMLi: An open-source library for modelling and inversion in geophysics. *Computers & Geosciences*, *109*, 106–123.
- Schreiber, L. (2010). Transport barriers made of cutin, suberin and associated waxes. *Trends in Plant Science*, *15*(10), 546–553. <https://doi.org/10.1016/j.tplants.2010.06.004>
- Seigel, H. O. (1959). Mathematical formulation and type curves for induced polarization. *Geophysics*, *24*(3), 547–565. <https://doi.org/10.1190/1.1438625>
- Tarasov, A., & Titov, K. (2013). On the use of the Cole-Cole equations in spectral induced polarization. *Geophysical Journal International*, *195*(1), 352–356. <https://doi.org/10.1093/gji/ggt251>
- Tavakkoli, E., Rengasamy, P., & McDonald, G. K. (2010). The response of barley to salinity stress differs between hydroponic and soil systems. *Functional Plant Biology*, *37*(7), 621. <https://doi.org/10.1071/FP09202>
- Teixeira, V. S., Krautschneider, W., & Montero-Rodriguez, J. J. (2018). Bioimpedance spectroscopy for characterization of healthy and cancerous tissues. In *2018 IEEE International Conference on Electrical Engineering and Photonics (EExPolytech)* (pp. 147–151). St. Petersburg: IEEE.
- Ulrich, C., & Slater, L. (2004). Induced polarization measurements on unsaturated, unconsolidated sands. *Geophysics*, *69*(3), 762–771. <https://doi.org/10.1190/1.1759462>
- Urban, J., Bequet, R., & Mainiero, R. (2011). Assessing the applicability of the earth impedance method for in situ studies of tree root systems. *Journal of Experimental Botany*, *62*(6), 1857–1869. <https://doi.org/10.1093/jxb/erq370>
- Volkov, A. G. E. d. (2006). *Plant electrophysiology: Theory and methods*. New York: Springer.
- Weigand, M. (2017). Time-lapse Cole-Cole decomposition routines. https://m-weigand.github.io/ccd_tools/doc_ccd/index.html.
- Weigand, M., & Kemna, A. (2016). Debye decomposition of time-lapse spectral induced polarisation data. *Computers Geosciences*, *86*, 34–45. <https://doi.org/10.1016/j.cageo.2015.09.021>
- Weller, A., & Slater, L. (2012). Salinity dependence of complex conductivity of unconsolidated and consolidated materials: Comparisons with electrical double layer models. *Geophysics*, *77*(5), D185–D198. <https://doi.org/10.1190/geo2012-0030.1>
- Zhang, M. I. N., Repo, T., Willison, J. H. M., & Sutinen, S. (1995). Electrical impedance analysis in plant tissues: On the biological meaning of Cole-Cole α in Scots pine needles. *European Biophysics Journal*, *24*(2). <https://doi.org/10.1007/BF00211405>
- Zhao, P. - F., Wang, Y. - Q., Yan, S. - X., Fan, L. i-F., Wang, Z. i-Y., Zhou, Q., Yao, J. - P., Cheng, Q., Wang, Z. -Y. i, & Huang, L. (2019). Electrical imaging of plant root zone: A review. *Computers and Electronics in Agriculture*, *167*, 105058. <https://doi.org/10.1016/j.compag.2019.105058>
- Zimmermann, H. M., & Steudle, E. (1998). Apoplastic transport across young maize roots: Effect of the exodermis. *Planta*, *206*(1), 7–19. <https://doi.org/10.1007/s004250050368>

How to cite this article: Peruzzo, L., Liu, X., Chou, C., Blancaflor, E. B., Zhao, H., Ma, X.-F., Mary, B., Iván, V., Weigand, M., & Wu, Y. Three-channel electrical impedance spectroscopy for field-scale root phenotyping. *Plant Phenome J.* 2021;4:e20021. <https://doi.org/10.1002/ppj2.20021>